Electronic transport through a quantum dot network

August Dorn,¹ Thomas Ihn,¹ Klaus Ensslin,¹ Werner Wegscheider,² and Max Bichler³
¹ Solid State Physics Laboratory, ETH Zürich, 8093 Zürich, Switzerland
² Institut für experimentelle und angewandte Physik, Universität Regensburg, Germany
³ Walter Schottky Institut, Technische Universität München, Germany
(Dated: August 28, 2018)

The conductance through a finite quantum dot network is studied as a function of inter-dot coupling. As the coupling is reduced, the system undergoes a transition from the antidot regime to the tight binding limit, where Coulomb resonances with on average increasing charging energies are observed. Percolation models are used to describe the conduction in the open and closed regime and contributions from different blockaded regions can be identified. A strong negative average magnetoresistance in the Coulomb blockade regime is in good quantitative agreement with theoretical predictions for magnetotunneling between individual quantum dots.

I. INTRODUCTION

Arrays of insulating islands in two-dimensional electron systems in the ballistic regime are often referred to as antidot lattices. 1,2 Features observed in the magnetoresistance include commensurability peaks corresponding to quasi pinned orbits around $1,4,9,\ldots$ antidos 3,4 and Aharonov-Bohm type oscillations superimposed on the first commensurability peak. 5,6 The search for an artificial band structure at B=0 T is still ongoing.

Here we present measurements on a finite array with a very small lattice constant of 120 nm, where the global electron density can be varied continuously with a metallic top gate. This allows us to monitor the transition from an antidot to a quantum dot array, that takes place when the electron density is reduced and the constrictions between neighboring antidots enter the tunneling regime. Our sample is special in the sense that the extremely small lattice constant raises the charging energies to well observable levels and ensures that the lattice enters the tunneling regime well before the leads go insulating.

In the following we primarily focus on electronic transport in the quantum dot network regime, which can be compared to conduction through granular or disordered materials. Related systems include arrays of metallic nano-crystals^{7,8,9,10,11}, layers of semiconductor quantum dots^{12,13}, porous silicon¹⁴, 3D arrays of semiconductor nanocrystals^{15,16} and organic molecular crystals¹⁷. However, unlike most experiments on macroscopic samples, we are able to tune the inter dot coupling continuously and resolve individual Coulomb resonances due to the mesoscopic dimensions of our system. The local and global properties of the network are investigated by measuring across different terminals and phase coherence is probed by applying a perpendicular magnetic field.

II. SAMPLE

Starting with a high quality GaAs/AlGaAs heterostructure hosting a two-dimensional electron system (2DES) 34 nm below the surface, we used AFM-

lithography to define the nanostructure under study. This patterning method relies on an atomic force microscope with a conducting tip to locally oxidize the surface of a GaAs heterostructure and thereby locally depleting the underlying 2DES (see Refs 18 and 19 for details). In this way a square lattice of 20×20 insulating islands with a lattice constant of a=120 nm was fabricated and enclosed by an insulating cavity with openings in the corners that serve as current and voltage leads (see inset Fig.1). Later a TiAu top gate was evaporated over the entire structure using a shadow mask technique.

III. MEASUREMENTS

At high electron densities clear commensurability peaks around 1 and 4 antidots appear with superimposed ballistic conductance fluctuations (see Fig. 1), compara-

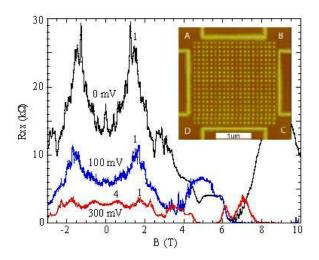


FIG. 1: Magnetoresistance measured from A to C across diagonal 1 at different top gate voltages at T=90 mK, commensurability peaks around 1 and 4 antidots are marked. Inset: AFM-micrograph of the antidot lattice and the enclosing cavity. Bright regions are oxidized and correspond to depletion in the underlying two-dimensional electron system.

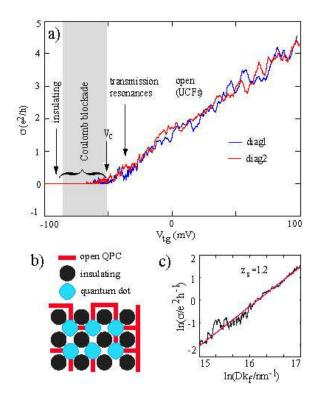


FIG. 2: (a) Conductance as a function of top gate voltage across diagonal 1(A-C) and diagonal 2(B-D) at T=90 mK. Bright regions are oxidized and correspond to depletion in the underlying 2DES. (b) Schematic of the lattice illustrating quantum dot formation and the bond percolation model. (c) Double logarithmic plot of the averaged conductance over $\Delta k_f = k_f - k_{fpc}$ with $k_{fpc} = k_f$ at P_c . The slope of the linear fit yields a value of $\zeta_{\sigma} = 1.2$.

ble to measurements taken on a similar sample with a larger lattice constant by Schuster et al.⁶. This indicates that despite the small period, we still have a very symmetric two-dimensional potential modulation. It is worth noting, that pronounced commensurability maxima in the magnetoresistance even occur for values exceeding the resistance quantum.

By applying suitable voltages to the top gate electrode, the electron sheet density in the 2DES can be tuned from about 2 to 5.5×10^{15} m⁻². The carrier density in the lattice is about 1.5×10^{15} m⁻² lower than in the unpatterned 2DES as determined from the Shubnikov–de Haas effect. Since the resistance in the leads is smaller than $h/2e^2$ down to top gate voltages below -100 mV it can be neglected in all measurements discussed here. Figure 2(a) shows the conductivity measured across diagonal 1 from corner A to C and across diagonal 2 from corner B to D as a function of top gate voltage at T=90 mK. As the voltage is lowered, the electron sheet density and the conductivity decrease until the Coulomb blockade regime is reached. This transition takes place at a top gate voltage of about -50.8 mV, marked by V_c in Fig. 2(a). Towards even lower voltages a series of on average decreas-

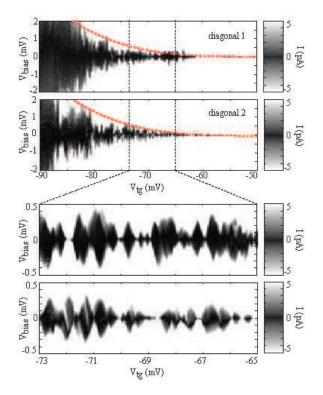


FIG. 3: Current as a function of top gate and bias voltage. White regions represent absolute current values above 5 pA. The upper two graphs are overview plots for diagonals 1 and 2, dashed lines are guides to the eye and correspond to a scaling exponent of about 3 with respect to k_F . The lower two graphs are blowups showing well defined Coulomb diamonds. All measurements were taken at a He bath temperature of 90 mK at B = 0 T.

ing Coulomb peaks is observed until conduction completely ceases below about -90 mV. It is worth pointing out, that the conductivity across both diagonals is very similar over the entire range of top gate voltages studied aside from mesoscopic fluctuations of the conductance caused by interference and interaction. This indicates the high symmetry and homogeneity of our sample. We would like to stress, that the physics in the ballistic antidot regime at high electron densities is in marked contrast to the quantum dot network regime close to and below V_c . In particular the linear transport characteristics of an antidot lattice and the classical ballistic trajectories responsible for the commensurability maxima give way to nonlinearities owing to Coulomb charging and magnetotunneling between individual localized states. During this transition the conductivity changes by several orders of magnitude.

In order to gain more insight into the electronic properties of the Coulomb blockade regime, we measured the current as a function of top gate and bias voltage. As can be seen in Fig. 3, blockade is lifted at sufficiently high bias voltages and clear 'Coulomb diamonds' are resolved. In contrast to analogous measurements on single

quantum dots, overlapping diamonds as well as streches in top gate voltage without Coulomb blockade are observed. This indicates the formation of a network with blockaded regions connected in series and in parallel. The charging energy for the individual resonances can be determined from the bias voltage maxima V_{max} at the tips of the Coulomb diamonds according to:

$$E_{charging} = eV_{max} = \frac{e^2}{C} + \Delta_N, \tag{1}$$

where C is the capacitance and Δ_N is the quantum mechanical single-particle energy spacing for the Nth state. Neglecting Δ_N , which makes a contribution of about 10% to the total energy, and applying a plate capacitor model, the area of the blockaded regions can be determined using:

$$C = \epsilon_0 \epsilon_{GaAs} \frac{A_{CB}}{d} \tag{2}$$

where A_{CB} is the area of the Coulomb blockaded region and d is the distance between 2DES and top gate. This leads to an average size of about 30 unit cells (or dots) at $V_{tg} = -60 \,\mathrm{mV}$ and about 4 unit cells at $V_{tg} = -80 \,\mathrm{mV}$, if the diameter of the insulating discs is set to 80 nm based on the oxide height profile.

IV. PERCOLATION ANALYSIS

In the following we apply percolation theory²⁰ to analyze these findings. This can be done by considering the conductance of the entire lattice as being dominated by the constrictions between neighboring insulating discs forming quantum point contacts (QPCs). The area enclosed by four insulating islands can then be viewed as a quantum dot or artificial atom with four terminals connecting it to its nearest neighbor quantum dots (see Fig. 2(b)). As the electron sheet density is reduced, the conductivity of the QPCs decreases until the last channel pinches off and the QPC goes insulating. Owing to small inhomogeneities inherent to the fabrication process and the presence of stray background charges, the closing of the QPCs will be a statistical process. In a classical picture, the QPCs can then be viewed as either conducting or broken resistors on a square bond-percolation lattice. Since the conductance staircase of a QPC can be approximated to be linear with respect to the Fermi wavenumber $k_F = \sqrt{2\pi n(V_{tq})}$, where $n(V_{tq})$ is the top gate voltage dependent electron sheet density in the lattice, this parameter is a natural choice for further analysis. In addition we identify the percolation threshold P_c for the open regime with $V_c = -50.8 \text{ mV}$ and assume the fraction of conducting bonds, or QPCs, P, to be proportional to $\Delta k_F = k_F(V_{tq}) - k_F(V_c)$. The exact relation depends on the width distribution of the QPCs, but close to the per-colation threshold $P_c=0.5,^{20}$ where half of the bonds are expected to be insulating, this is a reasonable assumption. This suggests a percolation transition with a characteristic scaling behavior of the type:²⁰

$$\sigma \propto (\Delta k_F)^{\zeta}, \quad \Delta k_F = k_F(V_{tq}) - k_F(V_c),$$
 (3)

where ζ is a critical exponent corresponding to a specific quantity. From a double logarithmic plot of the conductance averaged across both diagonals as a function of Δk_F , we extract a conductivity scaling exponent $\zeta_{\sigma} = 1.2 \pm 0.2$ in the open regime (Fig. 2(c)). This can be compared with the calculated value of 1.32 ± 0.02 (Ref. 21) for bond percolation in a classical square random resistor network, if phase coherence is neglected. Theoretical work describing a similar scenario has also been set forth by Meir²² in a model for the metal insulator transition in two dimensions.

In the Coulomb blockade regime, we follow the 'links, nodes, and blobs model' introduced by Stanly²³ and Coniglio²⁴. In this picture, the spanning network is decomposed into multiply connected 'blob bonds' and 'dangling bonds' forming 'blobs', that are in turn linked by individual 'cutting' bonds. In our system the blobs correspond to clusters of strongly coupled quantum dots that constitute the blockaded regions, while the 'cutting bonds' act as tunneling links. As the electron density is reduced, more and more QPCs pinch off and the clusters,

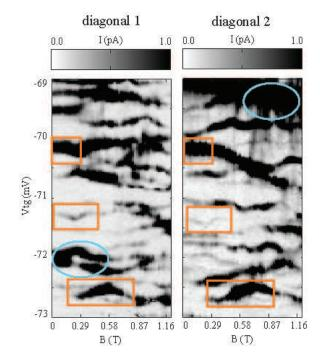


FIG. 4: Conductance as a function of top gate voltage and magnetic field across diagonals 1 and 2 at a He bath temperature of 90 mK. Boxes highlight similar features associated with the same blockaded regions, while ovals mark features unique to one diagonal.

or blobs, shrink, leading to higher charging energies. The envelope functions in Fig. 3 correspond to a size scaling exponent of about $\zeta_{CB}=3\pm1$ as a function of $-\Delta k_F^{38}$ which is comparable to theoretical calculations for the blob size scaling exponent $\xi_B=2.06-2.16$ (Ref.24) and the mean cluster size $\gamma=43/18\approx2.4$.

In order to make this interpretation more consistent, it might be more appropriate to consider a two stage process. First a QPC goes from open $(\sigma > 2e^2/h)$ to tunneling $(\sigma < 2e^2/h)$, before becoming practically insulating $(\sigma \sim 0)$. The first stage describes the transition from the open to the Coulomb blockaded regime, while the second one induces the transition from the Coulomb blockaded to an insulating state. The spanning cluster above $k_F(V_c)$ then consists of open QPCs, while the cutting bonds in Coulomb blockade are formed by QPCs in the tunneling regime. In either case the interpretation of the critical exponents should be viewed as tentative owing to the experimental uncertainty concerning the fraction P of open (tunneling) QPCs. We also point out, that a precise theoretical understanding of Coulomb blockade scaling that includes effects from clusters connected in series and in parallel is still outstanding.

Individual clusters of quantum dots in the network can be monitored by measuring the shift of the Coulomb peaks as a function of magnetic field across both diagonals (Fig. 4). Since the magnetic field dependent energy variation of a quantum state is related to the exact shape and symmetry of its wave function, this variation can be regarded as a fingerprint of a specific cluster. Similar features in Fig. 4 can be attributed to the same cluster being traversed by current flow across both diagonals, whereas differing features originate from clusters predominantly probed by transport across one of the two diagonals. This demonstrates, that transport is not dominated by a single quantum dot or small cluster close to one of the leads.

V. PHASE COHERENCE

Phase coherence across the spanning network was investigated by measuring the magnetoconductance as a function of top gate voltage (Fig. 5). The averaged magnetoconductance in the blockaded regime shows an increase with magnetic field by a factor of approximately 3, which is significantly higher than the value of 4/3 predicted by Alhassid²⁵ and measured by Folk et al.²⁶ for single quantum dots. This increase occurs on a magnetic field scale that corresponds to one flux quantum per unit cell and is consistent with a magnetotunnling effect proposed by Raikh and Glazmann²⁷ between elliptical 'electron lakes'.³⁹ They predict a low field magnetoresistance of the form:

$$\frac{\delta R(B)}{R(0)} \approx -\frac{B^2}{B_0^2} \tag{4}$$

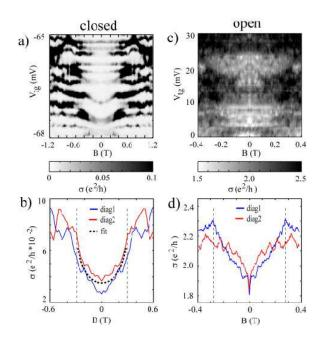


FIG. 5: (a) Conductance as a function of top gate voltage and magnetic field in the Coulomb blockade regime at $T=90\,\mathrm{mK}.$ A clear positive magnetoconductance for individual Coulomb peaks is observed. (b) Averaged magnetoconductance between -54 mV and -70 mV in steps of 0.02 mV. Dashed lines mark a flux quantum through the unit cell (290 mT) and a fit using equation 4. (c) Conductance as a function of top gate voltage and magnetic field in the open regime. (d) Averaged magnetoconductance between 30 and 0 mV in steps of 0.25 mV. Dashed lines mark a flux quantum through the unit cell (290 mT).

where B_0 depends on the details of the tunnel barrier, but is typically of the order of $h/e \cdot 1/d_1d_2$, d_1 and d_2 being the semiaxes of the two electron lakes. A best fit to the magnetoconductance averaged with respect to top gate voltage in the Coulomb blockade regime (dashed curve in Fig. 5(b)) yields a value of 2.2 T for B_0 . This corresponds to an average radius of about 40 nm, which is compatible with a single quantum dot confined to a unit cell. Evidence for this effect has also been reported by Voiskovskii and Pudalov²⁸, however without resolving the increase in conductivity of individual Coulomb peaks. Since Ref. 27 assumes perfect coherence within an electron lake and from the characteristic field scale of a flux quantum through a unit cell, we conclude, that the average dot radius can be considered as a lower bound for the phase coherence length in the Coulomb blockade regime. Remnants of this effect are still visible in the open regime (Fig. 5(d)), but weak localization is more prominent. From the dip around ± 5 mT we extract a phase coherence length of about 300 nm in the open regime.

In conclusion we have presented measurements on a multiply connected multi-terminal quantum dot network with tunable inter-dot coupling. Our sample is at a mesoscopic scale, where collaboratively Coulomb blockaded regions can be discriminated and related to macroscopic properties. For strong coupling close to the percolation threshold, a classical random resistor network model with superimposed quantum fluctuations can be applied until charge quantization becomes important in the tunneling regime. For weak coupling, Coulomb blockade domin ates resulting in the theoretically predicted 29,30,31 and experimentally observed 32,33 insulating state for $T\rightarrow 0$ with current onset above a bias voltage threshold and hopping transport at elevated temperatures. A strong parabolic decrease in average magnetoresistance in the Coulomb blockade regime around B=0 T, is in good quantitative agreement with theoretical predictions by Raikh and Glazman²⁷. These findings complement reports by Wiebe et al.³⁶, who performed scanning tunneling experiments, Ilani et al.³⁴, who obtained local potential information, and by Eytan et al.³⁵ who did scanning near field optical microscopy on two-dimensional percolating systems. We are able to quantitatively distinguish two length scales that are of fundamental importance for transport in the weak coupling regime. The first represents the decreasing area of the Coulomb blockaded clusters while the second one describes wavefunction localization to within the individual unit cells. Our measurements can also serve as an intuitive picture for the formation of the so-called 'Coulomb gap',³⁷ that opens up around the Fermi energy as a function of electron localization and Coulomb interactions.

We thank Y. Gefen, R. Leturcq, C. Marcus, and D. Pfannkuche for valuable discussions. This work was supported by the Schweizerischer Nationalfonds.

- ¹ K. Ensslin and P. M. Petroff, Phys. Rev. B **41**, 12307 (1990).
- ² R. Schuster and K. Ensslin, Adv. Solid State Phys. **34**, 195 (1994).
- D. Weiss, M. L. Roukes, A. Menschig, P. Grambow, K. v. Klitzing, and G. Weimann, Phys. Rev. Lett. 66, 2790 (1991).
- ⁴ R. Fleischmann, T. Geisel, R. Ketzmerick, Phys. Rev. Lett., **68**, 1367 (1992).
- ⁵ D. Weiss, K. Richter, A. Menschig, R. Bergmann, H. Schweizer, K. v. Klitzing, and G. Weimann, Phys. Rev. Lett. **70**, 4118 (1993).
- ⁶ R. Schuster, K. Ensslin, D. Wharam, S. Kühn, J. P. Kotthaus, G. Böhm, W. Klein, G. Tränkle, and G. Weimann, Phys. Rev. B 49, 8510 (1994).
- ⁷ R. Parthasarathy, X.-M. Lin, and H. M. Jaeger, Phys. Rev. Lett. **87**, 186807 (2001).
- ⁸ R. Parthasarathy, X.-M. Lin, K. Elteto, T. F. Rosenbaum, and H. M. Jaeger, Phys. Rev. Lett. **92**, 076801 (2004).
- ⁹ C. T. Black, C. B. Murray, R. L. Sandstrom, and S. Sun, Science **290**, 1131 (2000).
- ¹⁰ C. P. Collier, R. J. Saykally, J. J. Shiang, S. E. Henrichs, and J. R. Heath, Science 77, 1978 (1997).
- ¹¹ R. P. Andres, J. D. Bielefeld, J. I. Henderson, D. B. Janes, V. R. Kolagunta, C. P. Kubiak, W. J. Mahoney, Richard G. Osifchin Science 273, 1960 (1996).
- Min Ouyang and David D. Awschalom, Science 301, 1074 (2003).
- ¹³ N. Y. Morgan, C. A. Leatherdale, M. Drndic, M. V. Jarosz, M. A. Kastner, and M. Bawendi, Phys. Rev. B **66**, 075339 (2002).
- ¹⁴ B. Hamilton, J. Jacobs, D. A. Hill, R. F. Pettifer, D. Teehan, and L. T. Canham, Nature **393**, 443 (1998).
- ¹⁵ A. L. Roest, J. J. Kelly, D. Vanmaekelbergh, and E. A. Meulenkamp, Phys. Rev. Lett. 89, 036801 (2002).
- ¹⁶ D. Yu, C. Wang, P. Guyot-Sionnest, Science **300**, 1277 (2003).
- W. A. Schoonveld, J. Wildeman, D. Fichou, P. A. Bobbert, B. J. van Wees, and T, M. Klapwijk, Nature 404, 977 (2000).
- ¹⁸ A. Dorn, M. Sigrist, A. Fuhrer, T. Ihn, T. Heinzel, K. En-

- sslin, W. Wegscheider, and M. Bichler, Appl. Phys. Lett. 80, 252 (2002).
- ¹⁹ A. Fuhrer, A. Dorn, S. Lüscher, T. Heinzel, K. Ensslin, W. Wegscheider, M. Bichler, Superlattices and Microstructures, 31, 19, 2002.
- ²⁰ D. Stauffer and A. Aharony, Introduction to Percolation Theory (Taylor and Francis, London, 1992).
- ²¹ J. Bernasconi, Phys. Rev. B **18**, 2185 (1978).
- 22 Yigal Meir, Phys. Rev. Lett. ${\bf 83},\,3506$ (1999).
- ²³ H. E. Stanly, J. Phys. A **10**, L211, (1977).
- ²⁴ A. Coniglio, J. Phys. A **15**, 3829 (1982).
- ²⁵ Y. Alhassid, Rev. Mod. Phys. **72**, 895 (2000).
- ²⁶ J.A. Folk, C.M. Marcus, and J.S. Harris, Jr. Phys. Rev. Lett. 87, 206802 (2001).
- ²⁷ M. E. Raikh and L. I. Glazman, Phys. Rev. Lett. **75**, 128 (1995).
- ²⁸ A. E. Voiskovskii and V. M. Pudalov, JETP Lett. **62**, 947 (1995).
- ²⁹ A. A. Middelton and N. S. Wingreen, Phys. Rev. Lett. **71**, 3198 (1993).
- ³⁰ D. M. Kaplan, V. A. Sverdlov, and K. K. Likharev, Phys. Rev. B 68, 045321 (2003).
- ³¹ H.-O. Müller, D. A. Williams, and H. Mizuta, Jpn. J. Appl. Phys., Part 2 39, L723 (2000).
- ³² C. I. Duruöz, R. M. Clarke, C. M. Marcus, and J. S. Harris, Jr., Phys. Rev. Lett. **74**, 3237 (1995).
- ³³ C. Kurdak, A. J. Rimberg, T. R. Ho, and J. Clarke, Phys. Rev. B **57**, R6842 (1998).
- ³⁴ S. Ilani, A. Yacoby, D. Mahalu, and H. Shtrikman, Science 292 1354 (2001).
- ³⁵ G. Eytan, Y. Yayon, M. Rappaport, H. Shtrikman, and I. Bar-Joseph, Phys. Rev. Lett. 81, 1666 (1998).
- ³⁶ J. Wiebe, Chr. Meyer, J. Klijn, M. Morgenstern, and R. Wiesendanger, Phys. Rev. B 68, 041402 (2003).
- ³⁷ B. I. Shklovskii and A. L. Efros, Electronic properties of doped semiconductors, Springer, Berlin (1984).
- ³⁸ In the Coulomb blockade regime, k_F was determined by extrapolating the top gate voltage / electron sheet density dependence from the open regime.
- $^{39}\,$ This result should also hold for two chaotic quantum dots.